Green Chemistry

PAPER

View Article Online
View Journal | View Issue

Cite this: *Green Chem.*, 2026, **28**, 1713

A chemical–electrochemical cascading strategy for the efficient synthesis of 2,5-furandicarboxylic acid and its methyl ester from 2-furoic acid and CO_2

Ruizhi Li,†[a] Minling Zhong,†[a] Maitreyo Biswas,[b] Nan Jiang,[c] Arun Mannodi-Kanakkithodi *[b] and Yujie Sun *[a]

The electrocatalytic upgrading of biomass-derived furanics offers a sustainable route to high-value monomers for polymer manufacturing. Herein, we report a bromine-mediated electrochemical platform that converts 2-furoic acid and CO_2 into 2,5-furandicarboxylic acid (FDCA) and its dimethyl ester, dimethyl furan-2,5-carboxylate (FDME), under ambient conditions with faradaic efficiency exceeding 80% for the critical debromocarboxylation step. Specifically, our process involves sequential esterification and bromination of 2-furoic acid to yield methyl 5-bromofuran-2-carboxylate (MBFC), followed by electrochemical debromo-carboxylation on Ag to afford 5-(methoxycarbonyl)-2-furoic acid (MFCA). Subsequent hydrolysis or esterification would furnish the synthesis of FDCA and FDME, respectively. Comprehensive mechanistic studies, including *in situ* infrared spectroscopy, single-crystal facet analysis, and computational investigation, reveal that the key debromocarboxylation reaction proceeds through a two-electron transfer pathway, with Ag (100) and Ag (311) facets exhibiting the lowest activation barriers. Importantly, coupling cathodic debromocarboxylation with anodic bromide oxidation enables a paired electrolysis configuration in which the generated Br_2 can be recycled for substrate bromination, eliminating the need for a sacrificial anode and enhancing electron economy. Such an integrated, redox-balanced system establishes a scalable and environmentally benign route for converting renewable furanics and CO_2 into polymer precursors, highlighting the potential of bromine-mediated paired electrolysis for sustainable electrosynthetic manufacturing.

Received 23rd October 2025,
Accepted 15th December 2025

DOI: 10.1039/d5gc05661f

rsc.li/greenchem

Green foundation

1. We report a bromine-mediated electrochemical platform that converts 2-furoic acid and CO_2 into 2,5-furandicarboxylic acid (FDCA) and its dimethyl ester, dimethyl furan-2,5-carboxylate (FDME), under ambient conditions with faradaic efficiency exceeding 80% for the critical debromocarboxylation step.
2. We have collectively employed *in situ* infrared spectroscopy, single-crystal facet analysis, and computational investigation to reveal that the key debromocarboxylation reaction proceeds through a two-electron transfer pathway, with Ag (100) and Ag (311) facets exhibiting the lowest activation barriers.
3. Future research should focus on the integration of electrochemical synthesis with continuous product separation and electrolyte recycling in flow systems, thereby offering a transformative pathway toward scalable and sustainable electro-organic manufacturing.

Introduction

The depletion of fossil reserves and their associated environmental burdens have spurred the global pursuit of sustainable and renewable carbon sources.[1] Biomass carbohydrates, among the most abundant renewable materials, are widely recognized as pivotal feedstocks for green chemical manufacturing.[2] In particular, furan derivatives obtained *via* the dehydration of pentoses (C5) and hexoses (C6) have attracted considerable attention due to their structural versatility and potential for transformation into high-value chemicals.[3]

[a]*Department of Chemistry, University of Cincinnati, Cincinnati, OH 45221, USA. E-mail: yujie.sun@uc.edu*
[b]*School of Materials Engineering, Purdue University, West Lafayette, IN 47907, USA. E-mail: amannodi@purdue.edu*
[c]*Department of Chemistry and Chemical Engineering, Guizhou University, Guiyang, Guizhou, 550025, China*
†These authors contributed equally to this work.

Among these, 2,5-furandicarboxylic acid (FDCA) stands out as a premier bio-based platform molecule, designated by the U.S. Department of Energy as one of the "Top 12" value-added chemicals from biomass refineries.[4] For instance, FDCA can serve as a renewable replacement of terephthalic acid for the production of polyethylene furanoate (PEF),[5–8] a next-generation polymer that exhibits superior gas-barrier performance, higher mechanical strength, and improved thermal stability compared to conventional polyethylene terephthalate (PET). These advantages render PEF highly promising for food packaging and beverage container applications.[9–13] Nevertheless, the widespread commercialization of FDCA remains constrained by the limited efficiency and high cost of its current synthetic routes.

Since the pioneering synthesis of FDCA from mucic acid by Fittig and Heinzelmann in 1876 (Fig. 1a),[14] numerous synthetic strategies have been developed to access this valuable diacid from renewable resources. These approaches include dehydration of hexose derivatives (*e.g.*, galactaric acid and other aldaric acids),[15–17] oxidation of 5-hydroxymethylfurfural (HMF),[18–20] catalytic transformation of furan derivatives,[21] and biocatalytic oxidation routes.[22,23] Among them, HMF oxidation has emerged as the most established pathway to FDCA (Fig. 1b). However, the intrinsic instability of HMF complicates its preparation, purification, and oxidation, resulting in high processing costs and operational challenges.[24,25] These limitations have prompted increasing interest in more robust and readily available furan-based intermediates as alternative FDCA precursors.

2-Furoic acid, an industrially available and inexpensive platform molecule derived from the oxidation of furfural,[26] offers a particularly attractive route to FDCA. Produced from agricultural residues such as corn cobs, oat hulls, and sawdust, 2-furoic acid serves as a sustainable C5 feedstock that avoids competition with food resources.[27] Unlike HMF, 2-furoic acid exhibits excellent thermal and oxidative stability, facilitating storage and handling. However, its conversion to FDCA requires carbon chain extension from a five- to a six-carbon framework. Previous efforts (Fig. 1c) to achieve this transformation have included the Blanc reaction with formaldehyde, which generates 5-chloromethyl-2-furoic acid followed by multistep oxidation,[28] and the Henkel-type carboxylation under CO_2 at 250–400 °C, which operates under harsh conditions and suffers from poor selectivity.[29,30] Alternatively, high-temperature reactions in molten alkali metal salts can promote carbonate-mediated C–H carboxylation to FDCA,[31–34] while a separate strategy based on bromination of 2-furoic acid followed by Pd-catalyzed carbonylation also yields FDCA.[35–37]

Electrochemical synthesis has recently re-emerged as a powerful approach to sustainable chemical manufacturing, owing to its inherently mild reaction conditions, precise tunability, and direct compatibility with renewable electricity.[38] In this context, the electrocarboxylation of halogenated furan derivatives represents a promising pathway for constructing carbon-extended furanic acids from biomass feedstocks and CO_2. A recent report demonstrated the electrocarboxylation of methyl 5-bromofuran-2-carboxylate with CO_2 to form FDCA, underscoring the potential of electrochemical platforms in accessing bio-derived polymer precursors.[39] However, these systems typically exhibit limited faradaic efficiencies (often below 50%) and depend on sacrificial magnesium anodes, which generate metal contaminants, lower selectivity, and hinder process scalability.

To overcome these limitations, we sought to design an integrated, redox-balanced electrochemical platform capable of achieving high-efficiency carbon chain extension without the need for sacrificial metals. Here, we report a bromine-mediated paired electrolysis strategy that converts furoic acid and CO_2 into FDCA and its dimethyl ester FDME under ambient conditions (Fig. 1d). The process proceeds through sequential esterification, bromination, electrochemical debromocarboxylation, and subsequent hydrolysis or esterification, delivering overall faradaic efficiencies exceeding 80% for the key debromocarboxylation step. By coupling anodic bromide oxidation with cathodic debromocarboxylation, Br_2 generated at the anode can be recycled for substrate bromination, thereby eliminating the need for sacrificial anodes and enhancing both atom and electron economy. This integrated electrosynthetic approach establishes a sustainable route to polymer precursors from renewable furanics and CO_2, providing a generalizable blueprint for redox-balanced and circular electrochemical processes in green catalysis.

Results and discussion

We initiated this study by synthesizing methyl 5-bromofuran-2-carboxylate (MBFC) from furoic acid as the key electrochemical substrate (Scheme 1). Because the carboxylic acid group in furoic acid significantly influences the electron density of the furan ring, direct bromination under acidic conditions often leads to undesirable side reactions such as overbromination or ring cleavage. To suppress these pathways, furoic acid was first converted into its methyl ester (methyl furoate, MF) *via* acid-catalyzed esterification in methanol, affording a 90% isolated yield. Subsequent bromination of MF with 1.8 equivalents of Br_2 in acetic acid at 60 °C produced MBFC as a white solid in 77% yield. The purity and structural identity of both MF (Fig. S1 and S2) and MBFC (Fig. S3 and S4) were confirmed by NMR spectroscopy.

We next investigated the electrochemical debromocarboxylation of MBFC to produce 5-(methoxycarbonyl)furan-2-carboxylic acid (MFCA), the pivotal intermediate toward FDCA and FDME. To identify the optimal electrocatalyst, we screened a series of commercially available monometallic electrodes (Ag, Bi, Cu, Sn, and Zn) prepared by spray-coating catalyst inks onto carbon paper electrodes. Linear sweep voltammetry (LSV) was first conducted in CO_2-saturated acetonitrile (MeCN) containing 0.1 M tetrabutylammonium bromide (TBABr). MeCN was selected because it offers among the highest CO_2 solubilities of common organic solvents while maintaining relatively low toxicity, making it well suited for electrocarboxylation

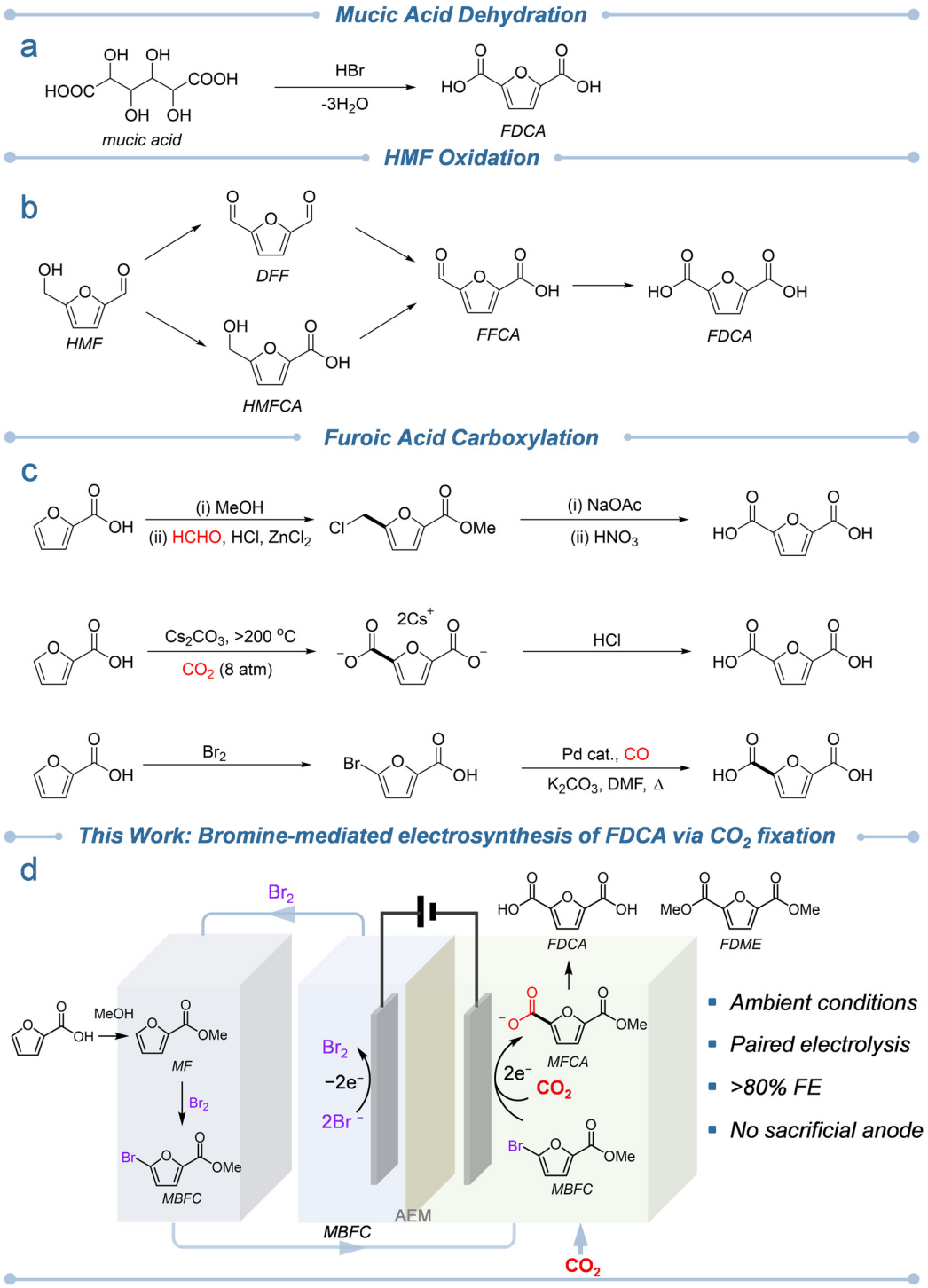

Fig. 1 Representative synthetic routes of 2,5-furandicarboxylic acid (FDCA) from (a) mucic acid dehydration. (b) HMF oxidation. (c) 2-Furoic acid carboxylation. (d) Bromine-mediated electrosynthesis of FDCA and FDME *via* CO_2 fixation (this work).

reactions.[40,41] In the absence of MBFC, negligible cathodic current was observed until potentials more negative than −1.6 V *vs.* Ag/AgCl (all reported potentials in this study are referenced *versus* Ag/AgCl unless noted otherwise), consistent with the onset of electrochemical CO_2 reduction. Upon the addition of 5 mM MBFC, the cathodic current increased sharply and shifted anodically, indicating an additional reduction process associated with debromocarboxylation. Among all tested metals, Ag exhibited the highest catalytic activity, delivering a current density of −5.8 mA cm^{-2} at −1.3 V, significantly outperforming the others across the potential range of −1.2 V to −1.6 V where CO_2 reduction remains negligible (Fig. S5). These

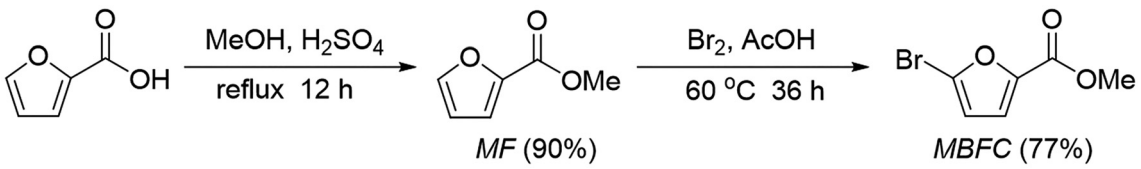

Scheme 1 Synthesis of MBFC from 2-furoic acid *via* esterification followed by bromination.

results identify Ag as the most effective electrocatalyst for promoting the selective electrochemical debromocarboxylation of MBFC, in agreement with previous studies on dehalocarboxylation of other substrates.[42–45]

The electrocatalytic behavior of Ag toward the debromocarboxylation of MBFC was further examined by cyclic voltammetry (CV) using Ag-decorated glassy carbon electrodes under various conditions. In CO_2-saturated MeCN containing 0.1 M TBABr, Ag displayed negligible current between −0.4 and −1.65 V, with a significant cathodic current increase observed only beyond −1.65 V, corresponding to direct electrochemical CO_2 reduction (CO_2RR) (Fig. 2a). Upon introducing 5 mM MBFC, the cathodic current increased substantially beginning at −1.1 V, accompanied by an irreversible reduction peak attributed to MBFC activation. The onset of this peak at a more positive potential than CO_2RR establishes a clear potential window in which selective debromocarboxylation proceeds without interference from competing CO_2 reduction. In parallel, bromide ions released during MBFC reduction were oxidized anodically to regenerate Br_2, which can be isolated and directly reused for substrate bromination. Integrating this anodic bromide oxidation with cathodic debromocarboxylation enables a paired electrolysis configuration that maximizes both atom economy and energy efficiency. This dual redox cycle, previously validated in our group,[46,47] forms the basis for a sustainable, closed-loop electrosynthetic platform.

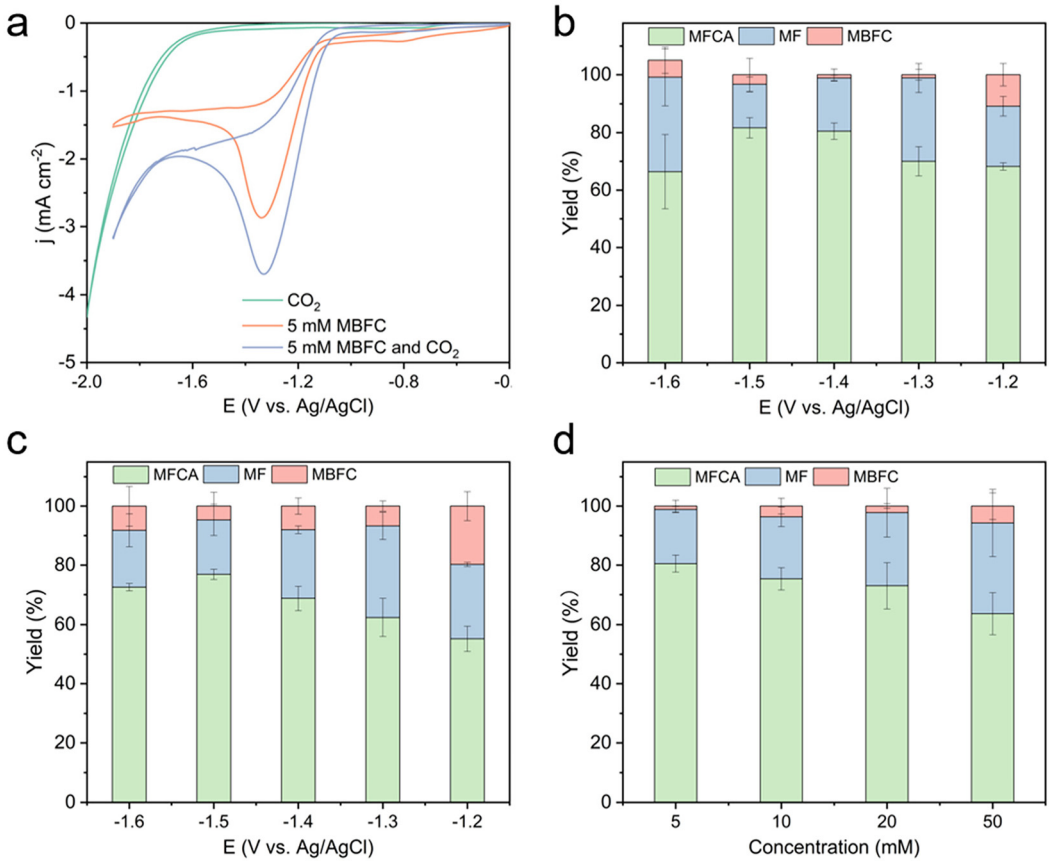

Fig. 2 (a) CV curves recorded at a scan rate of 20 mV s^{-1} in 0.1 M TBABr/MeCN using Ag-decorated glassy carbon electrode. (b) Yields of MFCA, MF and MBFC in 0.1 M TBABr/MeCN (5 mM MBFC) on Ag/CP electrode at different applied potentials after passing theoretical charge of 14.5C. (c) Yields of MFCA, MF and MBFC in 0.1 M TBABr/DMF (5 mM MBFC) on Ag/CP electrode at different applied potentials after passing theoretical charge of 14.5C. (d) Yields of MFCA, MF and MBFC in MeCN at −1.4 V *vs.* Ag/AgCl Ag/CP electrode under different concentrations of MBFC.

Guided by these electrochemical insights, we performed potential-dependent electrolysis of MBFC in a conventional H-cell to optimize product selectivity and faradaic efficiency. For each run, the theoretical charge (14.5C) corresponding to the two-electron process of 5 mM MBFC in 15 mL electrolyte was fully passed, allowing the yield to directly represent the faradaic efficiency. Product distributions were quantified by NMR spectroscopy and high-performance liquid chromatography (HPLC, Fig. S6–S10). The MFCA yield exhibited a volcano-type dependence on the applied potential (Fig. 2b), reaching a maximum of approximately 80% at −1.4 to −1.5 V. In contrast, constant–current electrolysis produced a lower maximum MFCA yield (~67%) (Fig. S11a), primarily due to potential drift from −1.2 V to −1.85 V (Fig. S11b), which entered the CO_2 reduction regime and hence diminished selectivity. These results underscore the critical importance of precise potential control in achieving highly selective electrochemical debromocarboxylation of MBFC.

After identifying −1.4 V as the optimal potential, we examined solvent effects and catalyst stability to further elucidate factors governing reaction selectivity. Solvent deprotonation has been reported to significantly influence electrochemical carboxylation efficiency;[48] however, comparable MFCA yields (~77%) were obtained in both MeCN and *N*,*N*-dimethylformamide (DMF) despite their markedly different deprotonation energetics (−153.9 and −82.2 kJ mol^{-1}, respectively) (Fig. 2c). This observation suggests that solvent deprotonation plays a negligible role in determining product selectivity within the studied potential range.

The durability of Ag/CP was assessed through eight consecutive electrolysis cycles conducted at −1.4 V. MFCA yields remained stable with only minor fluctuations, and chronoamperometric profiles were nearly identical across all runs (Fig. S12). Scanning electron microscopy (SEM, Fig. S13) and X-ray diffraction (XRD, Fig. S14) analyses confirmed that the Ag catalyst retained its morphology and crystallographic features after repeated operation, indicating excellent structural robustness under the applied electrochemical conditions.

Substrate concentration, a crucial factor influencing both mass transport and surface adsorption, was next investigated to assess its effect on product distribution. Chronoamperometric measurements were performed at −1.4 V while varying the MBFC concentration from 5 to 50 mM. Across this range, overall substrate conversion remained nearly constant after passing the theoretical charge, indicating that the reaction was not mass-transfer limited. However, the selectivity toward MFCA decreased from 80% to 64% as the MBFC concentration increased, while the yield of the byproduct MF rose correspondingly from 18% to 30% (Fig. 2d). This inverse relationship suggests that elevated substrate concentration favors undesired side reactions such as hydrodebromination. Maintaining a high $[CO_2]$/[MBFC] ratio is therefore essential for suppressing competing pathways and promoting selective carboxylation. These findings are consistent with prior electrocarboxylation studies,[49] reinforcing that the balance between substrate concentration and CO_2 availability critically determines reaction selectivity. Accordingly, the use of relatively diluted MBFC solutions should be viewed as an intentional strategy to maximize FE rather than as a fundamental synthetic limitation. Moreover, our system employs bromide oxidation at the anode instead of a sacrificial metal anode, thereby avoiding electrolyte contamination from metal cations, eliminating downstream metal recovery, and enabling long-term operation in flow-cell configurations.[50–54] Building on these advantages, we envisage that large-scale production can be achieved by integrating high-surface-area Ag architectures in flow cells,[55–58] which would maintain a high effective $[CO_2]$/[MBFC] ratio while processing substantially larger substrate quantities.

To gain deeper insight into the reduction pathway from MBFC to MFCA, we employed *in situ* attenuated total reflectance Fourier-transform infrared (ATR-FTIR) spectroscopy to monitor intermediate evolution during electrochemical debromocarboxylation on Ag (Fig. 3 and Fig. S15). Standard IR spectra of MBFC, MFCA, MF, and TBABr were first collected as references (Fig. S16a). Characteristic vibrational bands at 1725 and 1671 cm^{-1}, corresponding to the asymmetric C═O stretching modes of the carbonyl groups in MFCA, were used as diagnostic markers for product formation. During electrolysis at −1.4 V, these bands increased steadily in intensity over 60 minutes, confirming the progressive formation of MFCA. The band at 1671 cm^{-1}, associated with the –COOH stretching vibration, showed a particularly pronounced growth, providing direct evidence of carboxylation.[59–61] Additionally, a band at 1340 cm^{-1} corresponding to the symmetric stretching of carboxylate groups ($–COO^-$) became increasingly prominent, indicating accumulation of adsorbed carboxylate intermediates on the electrode surface.[62] Concurrently, a downward feature at 1593 cm^{-1}, attributed to C═C stretching within the furan ring, also suggested the gradual formation of MFCA.[63,64] *Ex situ* IR spectra recorded before and after electrolysis further con-

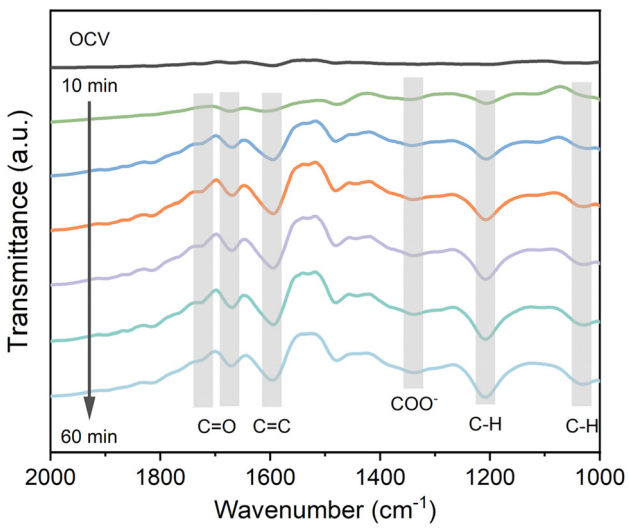

Fig. 3 Time-dependent *in situ* FTIR spectra of electrocatalytic debromocarboxylation of MBFC in MeCN over Ag at −1.4 V *vs.* Ag/AgCl.

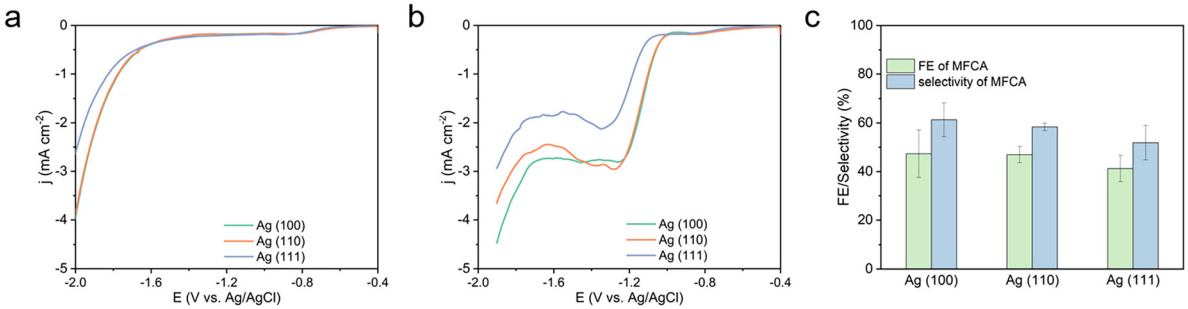

Fig. 4 (a) LSV curves recorded on single-crystal surfaces of Ag (100), Ag (110), and Ag (111) in CO_2 saturated 0.1 M TBABr/MeCN at a scan rate of 10 mV s^{-1}. (b) LSV curves recorded on single-crystal surfaces of Ag (100), Ag (110), and Ag (111) in CO_2 saturated 0.1 M TBABr/MeCN containing 5 mM MBFC at a scan rate of 10 mV s^{-1}. (c) FE and selectivity of MFCA formation in 0.1 M TBABr/MeCN with 5 mM MBFC at −1.4 V *vs.* Ag/AgCl after passing a total charge of 3C.

firmed the formation of MFCA through the appearance of the 1671 cm^{-1} band (Fig. S16b). Collectively, these *in situ* and *ex situ* IR spectroscopic results unambiguously demonstrate that MFCA is the dominant product generated during the electrochemical debromocarboxylation process of MBFC.

Silver, a face-centered cubic (FCC) metal, primarily exposes three low-index facets, (100), (110), and (111), that exhibit distinct electronic structures and adsorption behaviors toward reactive intermediates. To elucidate the facet-dependent activity in the electrochemical debromocarboxylation of MBFC, single-crystal Ag electrodes with defined exposed facets were employed as working electrodes. The corresponding X-ray diffraction (XRD) patterns confirmed the crystallographic integrity of these electrodes (Fig. S17). Although the (100) and (110) planes are not directly visible in the diffraction pattern due to forbidden FCC reflections, their presence could be inferred from the intensity of the (200) and (220) reflections, which are crystallographically aligned with these planes. Enhanced (200) and (220) intensities thus indicate greater exposure of Ag (100) and Ag (110) facets, respectively.[65]

Linear sweep voltammetry (LSV) conducted in CO_2-saturated electrolyte revealed that all Ag facets exhibited cathodic current onset beyond −1.65 V *versus* Ag/AgCl, consistent with CO_2 reduction behavior (Fig. 4a). Among these, Ag (100) and Ag (110) displayed markedly higher current densities than Ag (111), suggesting that these facets facilitate CO_2 activation more effectively. Open-circuit potential (OCP) measurements further demonstrated stronger MBFC adsorption on Ag (100),[66,67] evidenced by a ~40 mV potential decrease, significantly larger than those observed for Ag (110) (~15 mV) and Ag (111) (~20 mV) (Fig. S18). Corresponding LSVs in the presence of MBFC confirmed that Ag (100) and Ag (110) exhibited enhanced reduction currents relative to Ag (111) (Fig. 4b). Controlled potential electrolysis at −1.4 V *versus* Ag/AgCl revealed a consistent trend, with faradaic efficiency and product selectivity following the order Ag (100) > Ag (110) > Ag (111) (Fig. 4c). These results collectively demonstrate that electrochemical debromocarboxylation proceeds most efficiently on Ag (100) surfaces, underscoring the crucial role of facet engineering in optimizing catalytic performance.

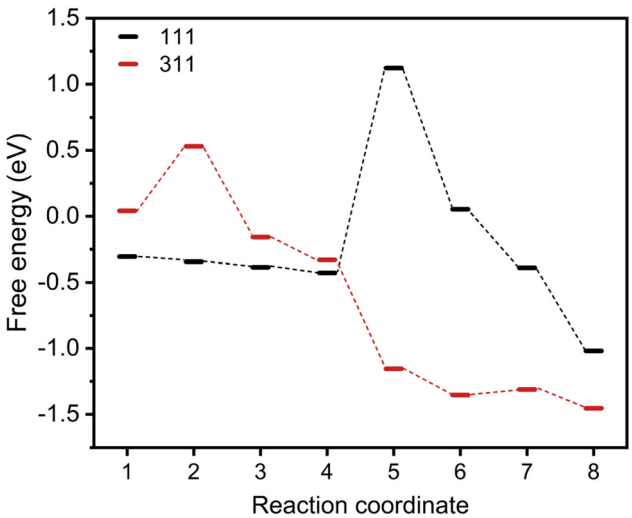

Fig. 5 The reaction energy profiles for electrochemical debromocarboxylation on Ag with different facets (111) and (311) MeCN, calculated using the climbing image nudged elastic band (Cl-NEB) method.

To further elucidate the facet-dependent activity of Ag in the electrochemical debromocarboxylation of MBFC, we performed density functional theory (DFT) calculations to evaluate the reaction energetics on different Ag surfaces (Fig. 5). Adsorption and reaction pathways were modeled on Ag (100), (110), and (111) surfaces under both vacuum and MeCN solvation environments. Nudged elastic band (NEB) calculations[68,69] were employed to map the minimum energy pathway for debromocarboxylation leading to MFCA. As shown in Fig. S19–S22, inclusion of the MeCN solvent environment significantly lowered the computed activation barriers relative to vacuum conditions (Fig. S23–S26), consistent with enhanced stabilization of polar intermediates in the electrochemical medium. Among the low-index facets, Ag (100) exhibited the lowest energy barrier (0.44 eV), followed by (110) (0.73 eV) and (111) (1.15 eV), indicating more favorable electron transfer and CO_2 incorporation on Ag (100). Since XRD analysis of the Ag/CP electrode also revealed partial exposure of the Ag (311) facet

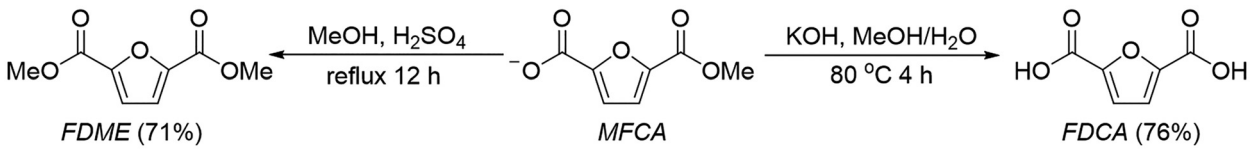

Scheme 2 Synthesis of FDME and FDCA from MFCA *via* esterification and hydrolysis, respectively.

(Fig. S14), it was therefore included in subsequent calculations. In the MeCN environment, Ag (311) showed an energy barrier of 0.53 eV while Ag (111) showed a much higher energy barrier of 1.13 eV (Fig. 5). Fig. S27 and S28 show the initial, final, and transition states (TS) for the reaction on the Ag (311) and Ag (111) facets respectively. These computational results corroborate the experimental findings and establish a clear structure–activity correlation: facets with higher coordination unsaturation, such as Ag (100) and Ag (311), facilitate MBFC adsorption and lower the activation barrier for C–Br bond cleavage, thereby enhancing catalytic performance.

Based on prior studies[70–74] and our combined experimental and computational findings, we propose a two-electron transfer mechanism for the electrochemical debromocarboxylation of MBFC on Ag surfaces. In the first step, MBFC undergoes a one-electron reduction at the cathode to generate a furan radical species along with adsorbed bromide ions on the Ag surface. This radical intermediate is subsequently reduced by a second electron to form a carbanion species, which then reacts with CO_2 to yield a surface-bound carboxylate intermediate. Protonation of this intermediate upon acid workup furnishes MFCA as the final product. This mechanistic sequence is supported by the *in situ* FTIR evidence of progressive carboxylate formation and the DFT-derived energy profiles showing that the rate-determining C–Br bond cleavage proceeds with the lowest barrier on Ag (100) and Ag (311) facets.

With these mechanistic insights established, we next converted MFCA into its corresponding diacid and diester derivatives, FDCA and FDME, to demonstrate the synthetic utility of this electrochemical platform (Scheme 2). Esterification of MFCA in methanol with catalytic H_2SO_4 under reflux for 12 h afforded FDME as a white solid in 71% isolated yield (Fig. S29 and S30). Alternatively, hydrolysis of MFCA with KOH in aqueous methanol at 80 °C followed by acidification and recrystallization produced FDCA in 76% yield (Fig. S31 and S32). These downstream transformations confirm that MFCA can serve as a versatile CO_2- and biomass-derived intermediate, enabling efficient access to two types of monomers for the manufacture of renewable polymers.

Conclusions

This study establishes a sustainable and efficient electrocatalytic route for synthesizing FDCA and FDME from the biomass-derived feedstock furoic acid. Our process integrates sequential esterification, bromination, electrochemical debromocarboxylation, and final hydrolysis or esterification, delivering high yields under mild conditions. Mechanistic investigations combining *in situ* FTIR spectroscopy, single-crystal facet analysis, and DFT calculations elucidate the critical role of Ag surface structure in governing the debromocarboxylation step. Specifically, Ag (100) and Ag (311) facets exhibit the lowest activation barriers for C–Br bond cleavage and CO_2 incorporation, rationalizing their superior activity and selectivity. Overall, this work demonstrates a mechanistically informed strategy for integrating biomass valorization with CO_2 utilization, advancing the broader goal of sustainable electrosynthetic manufacturing.

Methods

Details regarding the methods can be found in the SI.

Author contributions

Ruizhi Li: investigation, data curation, writing, formal analysis; Minling Zhong: investigation, data curation, writing, formal analysis; Maitreyo Biswas: computation; Nan Jiang: investigation; Arun Mannodi-Kanakkithodi: computation, funding acquisition; Yujie Sun: conceptualization, supervision, writing – review & editing, funding acquisition, resources, project administration.

Conflicts of interest

The authors declare no competing interests.

Data availability

The relevant experimental and characterization data are available in the article and the supplementary information (SI). Supplementary information: experimental details, characterization data (NMR, SEM, XRD, *etc.*), electrochemical results, and computational details. See DOI: https://doi.org/10.1039/d5gc05661f.

Acknowledgements

Y. S. and A. M. K. acknowledge the financial support of the US National Science Foundation (CHE 2328176).

References

1 N. Armaroli and V. Balzani, *Angew. Chem., Int. Ed.*, 2007, **46**, 52–66.
2 A. Corma, S. Iborra and A. Velty, *Chem. Rev.*, 2007, **107**, 2411–2502.
3 Y. Kwon, K. J. P. Schouten, J. C. van der Waal, E. de Jong and M. T. M. Koper, *ACS Catal.*, 2016, **6**, 6704–6717.
4 T. Werpy, G. Petersen, A. Aden, J. Bozell, J. Holladay, J. White, A. Manheim, D. Eliot, L. Lasure and S. Jones, *Top Value Added Chemicals from Biomass. Vol. 1. Results of Screening for Potential Candidates from Sugars and Synthesis Gas*, U. S. Department of Energy Report. Pacific Northwest National Laboratory/U.S. Department of Energy, Oak Ridge, TN, 2004.
5 F. Ye, S. Zhang, Q. Cheng, Y. Long, D. Liu, R. Paul, Y. Fang, Y. Su, L. Qu, L. Dai and C. Hu, *Nat. Commun.*, 2023, **14**, 2040.
6 D. Lei, K. Yu, M. R. Li, Y. Wang, Q. Wang, T. Liu, P. Liu, L. L. Lou, G. Wang and S. Liu, *ACS Catal.*, 2017, **7**, 421–432.
7 C. Wang, Y. Wu, A. Bodach, M. L. Krebs, W. Schuhmann and F. Schüth, *Angew. Chem., Int. Ed.*, 2023, **62**, e202215804.
8 Z. Zhang and K. Deng, *ACS Catal.*, 2015, **5**, 6529–6544.
9 R. J. van Putten, J. C. van der Waal, E. de Jong, C. B. Rasrendra, H. J. Heeres and J. G. de Vries, *Chem. Rev.*, 2013, **113**, 1499–1597.
10 S. Barwe, J. Weidner, S. Cychy, D. M. Morales, S. Dieckhöfer, D. Hiltrop, J. Masa, M. Muhler and W. Schuhmann, *Angew. Chem., Int. Ed.*, 2018, **57**, 11460–11464.
11 D. Chen, Y. Ding, X. Cao, L. Wang, H. Lee, G. Lin, W. Li, G. Ding and L. Sun, *Angew. Chem., Int. Ed.*, 2023, **62**, e202309478.
12 J. Iglesias, I. Martínez-Salazar, P. Maireles-Torres, D. M. Alonso, D. R. Mariscal and M. L. Granados, *Chem. Soc. Rev.*, 2020, **49**, 5704–5771.
13 N. Poulopoulou, N. Kasmi, M. Siampani, Z. N. Terzopoulou, D. N. Bikiaris, D. S. Achilias, D. G. Papageorgiou and G. Z. Papageorgiou, *Polymers*, 2019, **11**, 556.
14 R. Fittig and H. Heinzelmann, *Chem. Ber.*, 1876, **9**, 1198.
15 N. van Strien, S. Rautiainen, M. Asikainen, D. A. Thomas, J. Linnekoski, K. Niemelä and A. Harlin, *Green Chem.*, 2020, **22**, 8271–8277.
16 G. Trapasso, M. Annatelli, D. D. Torre and F. Aricò, *Green Chem.*, 2022, **24**, 2766–2771.
17 M. Annatelli, J. E. Sánchez-Velandia, G. Mazzi, S. V. Pandeirada, D. Giannakoudakis, S. Rautiainen, A. Esposito, S. Thiyagarajan, A. Richel, K. S. Triantafyllidis, T. Robert, N. Guigo, A. F. Sousa, E. García-Verdugo and F. Aricò, *Green Chem.*, 2024, **26**, 8894–8941.
18 B. You, N. Jiang, X. Liu and Y. Sun, *Angew. Chem., Int. Ed.*, 2016, **55**, 9913–9917.
19 B. You, X. Liu, N. Jiang and Y. Sun, *J. Am. Chem. Soc.*, 2016, **138**, 13639–13646.
20 D. J. Aranha and P. R. Gogate, *Ind. Eng. Chem. Res.*, 2023, **62**, 3053–3078.
21 X. Zhang, S. Xu, Q. Li, G. Zhou and H. Xia, *RSC Adv.*, 2021, **11**, 27042–27058.
22 K. A. Payne, S. A. Marshall, K. Fisher, M. J. Cliff, D. M. Cannas, C. Yan, D. J. Heyes, D. A. Parker, I. Larrosa and D. Leys, *ACS Catal.*, 2019, **9**, 2854–2865.
23 N. Li and M. H. Zong, *ACS Catal.*, 2022, **12**, 10080–10114.
24 C. Rosenfeld, J. Konnerth, W. Sailer-Kronlachner, P. Solt, T. Rosenau and H. W. van Herwijnen, *ChemSusChem*, 2020, **13**, 3544–3564.
25 A. N. Golysheva, D. A. Kolykhalov and B. Y. Karlinskii, *Korean J. Chem. Eng.*, 2025, **42**, 483–504.
26 N. Jiang, X. Liu, J. Dong, B. You, X. Liu and Y. Sun, *ChemNanoMat*, 2017, **3**, 491–495.
27 K. J. Zeitsch, *The chemistry and technology of furfural and its many by-products*, Elsevier, 2000, vol. 13.
28 G. Gonis and E. D. Amstutz, *J. Org. Chem.*, 1962, **27**, 2946–2947.
29 T. Pan, J. Deng, Q. Xu, Y. Zuo, Q. X. Guo and Y. Fu, *ChemSusChem*, 2013, **6**, 47–50.
30 S. Thiyagarajan, A. Pukin, J. van Haveren, M. Lutz and D. S. van Es, *RSC Adv.*, 2013, **3**, 15678–15686.
31 R. Fischer and M. Fišerová, *ARKIVOC*, 2013, 405–412.
32 A. Banerjee, G. R. Dick, T. Yoshino and M. W. Kanan, *Nature*, 2016, **531**, 215–219.
33 G. R. Dick, A. D. Frankhouser, A. Banerjee and M. W. Kanan, *Green Chem.*, 2017, **19**, 2966–2972.
34 X. Han, Y. Wang, G. Liu, M. Wang, C. Guo and J. Shen, *J. CO_2 Util.*, 2023, **75**, 102572.
35 G. Shen, S. Zhang, Y. Lei, Z. Chen and G. Yin, *Mol. Catal.*, 2018, **455**, 204–209.
36 G. Shen, J. Shi, Y. Lei, C. Fu, Z. Chen, B. Andrioletti and G. Yin, *Ind. Eng. Chem. Res.*, 2019, **58**, 22951–22957.
37 Y. Q. Yao, K. C. Zhao, Y. Y. Zhuang, X. C. Chen, Y. Lu and Y. Liu, *ChemistryOpen*, 2022, **11**, e202100301.
38 F. W. Lucas, R. G. Grim, S. A. Tacey, C. A. Downes, J. Hasse, A. M. Roman, C. A. Farberow, J. A. Schaidle and A. Holewinski, *ACS Energy Lett.*, 2021, **6**, 1205–1270.
39 M. Y. Lee, J. W. Koo, J. H. Jang, Y. I. Jo, J. B. Yeo, J. S. Hong, J. H. Kim, S. Choi and K. T. Nam, *ACS Sustainable Chem. Eng.*, 2025, **13**, 2845–2852.
40 M. M. Anouti, Y. R. Dougassa, C. Tessier, L. El Ouatani and J. Jacquemin, *J. Chem. Thermodyn.*, 2012, **50**, 71–79.
41 M. König, J. Vaes, E. Klemm and D. Pant, *iScience*, 2019, **19**, 135–160.
42 C. Durante, A. A. Isse, F. Todesco and A. Gennaro, *J. Electrochem. Soc.*, 2013, **160**, G3073–G3079.
43 O. Scialdone, A. Galia, G. Errante, A. A. Isse, A. Gennaro and G. Filardo, *Electrochim. Acta*, 2008, **53**, 2514–2528.
44 H. P. Yang, H. W. Zhang, Y. Wu, L. D. Fan, X. Y. Chai, Q. L. Zhang, J. H. Liu and C. X. He, *ChemSusChem*, 2018, **11**, 3905–3910.
45 P. P. Luo, Y. T. Zhang, B. L. Chen, S. X. Yu, H. W. Zhou, K. G. Qu, Y. X. Kong, X. Q. Huang, X. X. Zhang and J. X. Lu, *Catalysts*, 2017, **7**, 274.

46 X. Shang, X. Liu and Y. Sun, *Green Chem.*, 2021, **23**, 2037–2043.
47 M. Zhong, F. Wang, G. Han, S. Yuan, G. Li, D. E. Jiang and Y. Sun, Chem. Sci., 2025, DOI: 10.1039/D5SC05956A, Advance Article.
48 N. Corbin, G. P. Junor, T. N. Ton, R. J. Baker and K. Manthiram, *J. Am. Chem. Soc.*, 2023, **145**, 1740–1748.
49 J. J. Medvedev, X. V. Medvedeva, F. Li, T. A. Zienchuk and A. Klinkova, *ACS Sustainable Chem. Eng.*, 2019, **7**, 19631–19639.
50 H. P. Yang, Q. Lin, H. W. Zhang, G. D. Li, L. D. Fan, X. Y. Chai, Q. L. Zhang, J. H. Liu and C. X. He, *Chem. Commun.*, 2018, **54**, 4108–4111.
51 T. N. Ton, R. J. Baker and K. Manthiram, *J. Catal.*, 2024, **432**, 115371.
52 S. D. Ware, W. Zhang, W. Guan, S. Lin and K. A. See, *Chem. Sci.*, 2024, **15**, 5814–5831.
53 W. Zhang, W. Guan, Y. Wang, S. Lin and K. A. See, *Chem. Sci.*, 2023, **14**, 13108–13118.
54 Y. Li, L. Wen and W. Guo, *Chem. Soc. Rev.*, 2023, **52**, 1168–1188.
55 D. Iglesias, C. Tinajero, S. Marchetti, I. Roppolo, M. Zanatta and V. Sans, *Green Chem.*, 2023, **25**, 9934–9940.
56 Y. Naito, Y. Nakamura, N. Shida, H. Senboku, K. Tanaka and M. Atobe, *J. Org. Chem.*, 2021, **86**, 15953–15960.
57 Y. Qu, C. Tsuneishi, H. Tateno, Y. Matsumura and M. Atobe, *React. Chem. Eng.*, 2017, **2**, 871–875.
58 Y. Naito, M. Kondo, Y. Nakamura, N. Shida, K. Ishikawa, T. Washio, S. Takizawa and M. Atobe, *Chem. Commun.*, 2022, **58**, 3893–3896.
59 J. Wu, L. Xu, Y. Li, C. Dong, Y. Lu, T. T. T. Nga, Z. Kong, S. Li, Y. Zou and S. Wang, *J. Am. Chem. Soc.*, 2022, **144**, 23649–23656.
60 G. Fu, X. Kang, Y. Zhang, Y. Guo, Z. Li, J. Liu, L. Wang, J. Zhang, X. Z. Fu and J. L. Luo, *Nat. Commun.*, 2023, **14**, 8395.
61 J. Mao, D. Wang, C. Zhang, Y. Xie, Q. Song, B. Zhang, Y. Lou, C. Pan, J. Zhang, Y. Zhang and Y. Zhu, *Chem Catal.*, 2025, **5**, 101415.
62 D. Chen, W. Li, J. Liu and L. Sun, *Energy Environ. Sci.*, 2025, **18**, 3120–3128.
63 L. Chen, C. Yu, X. Song, J. Dong, J. Mu and J. Qiu, *Nat. Commun.*, 2024, **15**, 8072.
64 L. Zhao, Z. Lv, Y. Shi, S. Zhou, Y. Liu, J. Han, Q. Zhang, J. Lai and L. Wang, *Energy Environ. Sci.*, 2024, **17**, 770–779.
65 D. Qu, N. Jiang and Y. Sun, *J. Mater. Chem. A*, 2025, **13**, 22492–22503.
66 P. Zhou, X. Lv, S. Tao, J. Wu, H. Wang, X. Wei, T. Wang, B. Zhou, Y. Lu, T. Frauenheim, X. Fu, S. Wang and Y. Zou, *Adv. Mater.*, 2022, **34**, 2204089.
67 L. Zhang, Y. Liu, L. Li, T. Wu, Q. Wu, J. Z. Y. Seow, X. Lin, S. Sun, L. Tannesia, K. Tang, D. Shao, S. Xi, X. Guo and Z. J. Xu, *Energy Environ. Sci.*, 2025, **18**, 5622–5631.
68 G. Henkelman, B. P. Uberuaga and H. Jónsson, *J. Chem. Phys.*, 2000, **113**, 9901–9904.
69 V. Ásgeirsson, B. O. Birgisson, R. Bjornsson, U. Becker, F. Neese, C. Riplinger and H. Jónsson, *J. Chem. Theory Comput.*, 2021, **17**, 4929–4945.
70 G. Q. Sun, L. L. Liao, C. K. Ran, J. H. Ye and D. G. Yu, *Acc. Chem. Res.*, 2024, **57**, 2728–2745.
71 N. Corbin, D. T. Yang, N. Lazouski, K. Steinberg and K. Manthiram, *Chem. Sci.*, 2021, **12**, 12365–12376.
72 C. K. Ran, L. L. Liao, T. Y. Gao, Y. Y. Gui and D. G. Yu, *Curr. Opin. Green Sustainable Chem.*, 2021, **32**, 100525.
73 A. A. Isse, P. R. Mussini and A. Gennaro, *J. Phys. Chem. C*, 2009, **113**, 14983–14992.
74 A. A. Isse, C. Durante and A. Gennaro, *Electrochem. Commun.*, 2011, **13**, 810–813.